Deep Whole-Body Control: Learning a Unified Policy for Manipulation and Locomotion

Zipeng Fu[*†] **Xuxin Cheng**[*] **Deepak Pathak**
Carnegie Mellon University

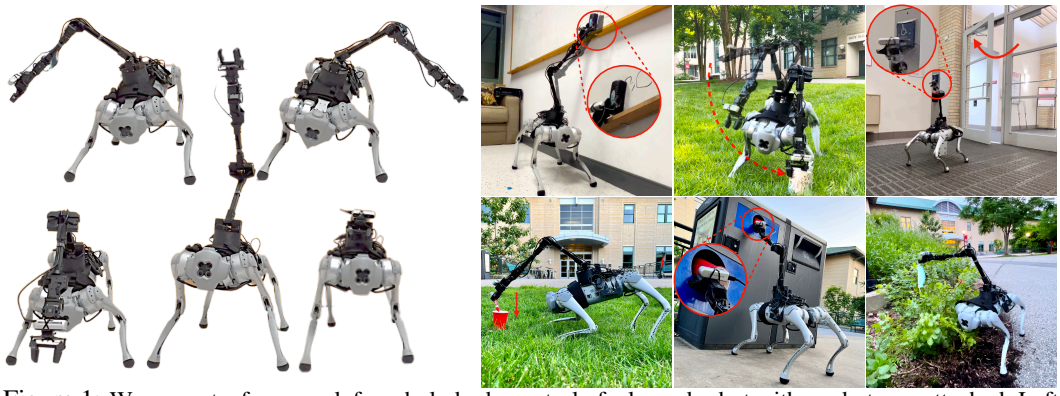

Figure 1: We present a framework for whole-body control of a legged robot with a robot arm attached. Left half shows how whole-body control achieves larger workspace by leg bending and stretching. Right half shows different real-world tasks, including wiping whiteboard, picking up a cup, pressing door-open buttons, placing, throwing a cup into a garbage bin and picking in clustered environments. Videos are here.

Abstract: An attached arm can significantly increase the applicability of legged robots to several mobile manipulation tasks that are not possible for the wheeled or tracked counterparts. The standard hierarchical control pipeline for such legged manipulators is to decouple the controller into that of manipulation and locomotion. However, this is ineffective. It requires immense engineering to support coordination between the arm and legs, and error can propagate across modules causing non-smooth unnatural motions. It is also biological implausible given evidence for strong motor synergies across limbs. In this work, we propose to learn a unified policy for whole-body control of a legged manipulator using reinforcement learning. We propose Regularized Online Adaptation to bridge the Sim2Real gap for high-DoF control, and Advantage Mixing exploiting the causal dependency in the action space to overcome local minima during training the whole-body system. We also present a simple design for a low-cost legged manipulator, and find that our unified policy can demonstrate dynamic and agile behaviors across several task setups. Videos are at https://maniploco.github.io

Keywords: Mobile Manipulation, Whole-Body Control, Legged Locomotion

1 Introduction

Locomotion has seen impressive performance in the last decade with results in challenging outdoor and indoor terrains, otherwise unreachable by their wheeled or tracked counterparts. However, there are strong limitations to what a legged-only robot can achieve since, besides visual inspection, even the most basic everyday tasks require some form of manipulation. This has led to immense progress in general-purpose legged manipulators primarily achieved through physical modeling of dynamics [1, 2, 3, 4, 5, 6]. However, modeling a legged robot with attached arm is a dynamic, high-DoF, and non-smooth control problem, requiring substantial domain expertise and engineering effort on the part of the designer. The control frameworks are often hierarchical with simplified

[*]equal contribution, [†]Zipeng Fu is now at Stanford University

6th Conference on Robot Learning (CoRL 2022), Auckland, New Zealand.

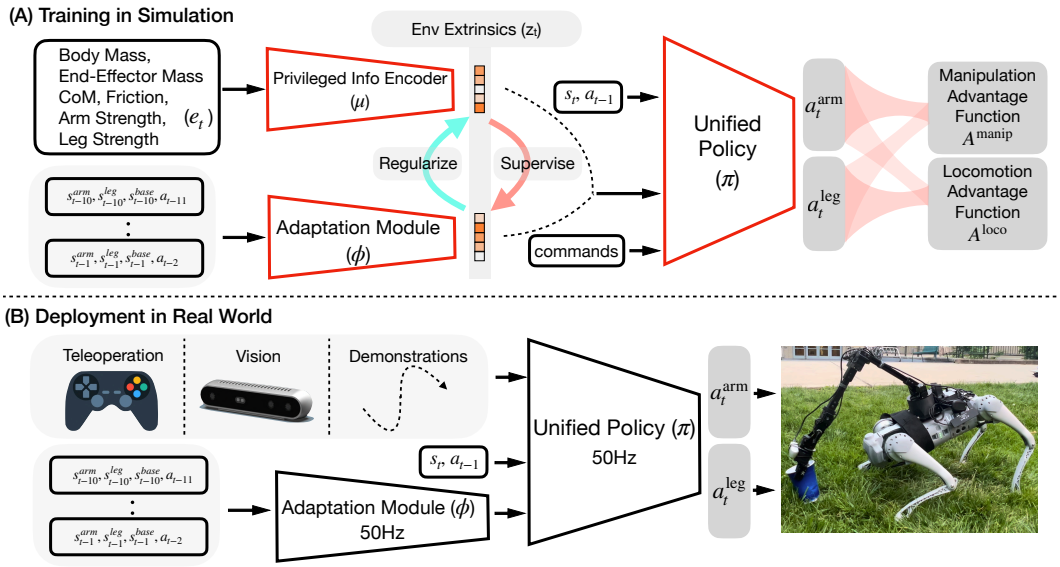

Figure 2: Whole-body control framework. During training, a unified policy is learned by conditioned on environment extrinsics. During deployment, the adaptation module is reused without any real-world fine-tuning. The robot can be commanded in various modes including teleoperation, vision and demonstration replay.

models at higher levels [7], thus limited to operating in constrained settings. Hence, there has been increasing interest in approaching this problem via reinforcement learning (RL) which could help lower the engineering burden while being able to generalize to diverse scenarios.

However, recent learning-based approaches for legged mobile manipulators [8] have also followed their model-based counterparts [9, 10] by using hierarchical models in a semi-coupled fashion to control the legs and arm. This is ineffective due to several practical reasons including lack of coordination between the arm and legs, error propagation across modules, and slow, non-smooth and unnatural motions. Furthermore, it is far from the whole-body motor control in humans where studies suggest strong coordination among limbs. In fact, the control of hands and legs is so tied together that they form low-dimension synergies, as outlined over 70 years ago in a seminal series of writings by Russian physiologist Nikolai Bernstein [11, 12, 13]. Perhaps the simplest example is how it is hard for humans to move one arm and the corresponding leg in different motions while standing. The whole-body control should not only allow coordination but also extend the capabilities of the individual parts. For instance, our robot bends or stretches its legs with the movement of the arm to extend the reach of the end-effector as shown in Figure 1.

Unlike legged locomotion, it is not straightforward to scale the standard RL paradigm of training the policies in simulation and then transfer to the real world due to several challenges with whole-body control. (a) *High-DoF control*: Our robot shown in Figure 3 has total 19 degrees of freedom. This problem is exacerbated in legged manipulators because the control is dynamic, continuous and high-frequency, which leads to an exponentially large search space even in few seconds of trajectory. (b) *Conflicting objectives and local minima*: Consider when the arm tilts to the right, the robot needs to change the walking gait to account for the weight balance. This curbs the locomotion abilities and makes training prone to learn only one mode (manipulation or locomotion) well. (c) *Dependency*: Consider picking an object on the ground, the end-effector of the arm needs support from the torso by bending legs. This means the absolute performance of manipulation is bounded until legs can adapt.

In this work, we present both a hardware setup for customized low-cost fully untethered legged manipulators and a method for learning one unified policy to control and coordinate both legs and arm, which is compatible with diverse operating modes as shown in Figure 1. We use our unified policy for whole-body control, i.e. to control the joints of the quadruped legs as well as the manipulator to simultaneously take the arm end-effector to desired poses and command the quadruped to move in desired velocities. The key insights of the method are that we can exploit the causal structure in action space with respect to manipulation and locomotion to stabilize and speed up learning, and

	Command Following ($r_{\text{following}}$)	Energy (r_{energy})	Alive (r_{alive})
r^{manip}	$0.5 \cdot e^{-\|[p,o]-[p^{\text{cmd}},o^{\text{cmd}}]\|_1}$	$-0.004 \cdot \sum_{j \in \text{arm joints}} \|\tau_j \dot{q}_j\|$	0
r^{loco}	$-0.5 \cdot \|v_x - v_x^{\text{cmd}}\| + 0.15 \cdot e^{-\|\omega_{\text{yaw}} - \omega_{\text{yaw}}^{\text{cmd}}\|}$	$-0.00005 \cdot \sum_{i \in \text{leg joints}} \|\tau_i \dot{q}_i\|^2$	$0.2 + 0.5 \cdot v_x^{\text{cmd}}$

Table 1: Both manipulation and locomotion rewards follow: $r_{\text{following}} + r_{\text{energy}} + r_{\text{alive}}$, which encourages command following while penalizes positive mechanical energy consumption to enable smooth motion [17]. Denote forward base linear velocity v_x, yaw angular base velocity ω_{yaw}, torque τ, joint angle velocity $\dot{q}$.

adding regularization to domain adaptation bridges the gap between simulation with full states and real world with only partial observations.

We perform evaluation on our proposed legged manipulator. Despite immense progress, there exists no easy-to-use legged manipulator for academic labs. Most publicized robot is Spot Arm from Boston Dynamics [14], but the robot comes with pre-designed controllers that cannot be changed. Another example is the ANYmal robot with a custom arm [8] from ANYBotics. Notably, both these hardware setups are expensive (more than 100K USD). We implement a simple design of low-cost legged Go1 robot [15] with low-cost arm on top (hardware costs 6K USD). Our legged manipulator can run fully untethered with modest on-board compute. We show the effectiveness of our learned whole-body controller for teleoperation, vision-guided control as well as open-loop control setup across tasks such as picking objects, throwing garbage, pressing buttons on walls etc. Our robot exhibits **dynamic** and **agile** leg-arm coordinated motions as shown in videos at https://maniploco.github.io.

2 Method: A Unified Policy for Coordinated Manipulation and Locomotion

We formulate the unified policy π as one neural network where the inputs are current base state $s_t^{\text{base}} \in \mathbb{R}^5$ (row, pitch, and base angular velocities), arm state $s_t^{\text{arm}} \in \mathbb{R}^{12}$ (joint position and velocity of each arm joint), leg state $s_t^{\text{leg}} \in \mathbb{R}^{28}$ (joint position and velocity of each leg joint, and foot contact indicators), last action $a_{t-1} \in \mathbb{R}^{18}$, end-effector position and orientation command $[p^{\text{cmd}}, o^{\text{cmd}}] \in \mathbb{SE}(3)$, base velocity command $[v_x^{\text{cmd}}, \omega_{\text{yaw}}^{\text{cmd}}]$, and environment extrinsics $z_t \in \mathbb{R}^{20}$ (details in Section 2.2). The policy outputs target arm joint position $a_t^{\text{arm}} \in \mathbb{R}^6$ and target leg joint position $a_t^{\text{leg}} \in \mathbb{R}^{12}$, which are subsequently converted to torques using PD controllers. We use joint-space position control for both legs and the arm. As opposed to operational space control of the arm, joint-space control enables learning to avoid self-collision and smaller Sim-to-Real gap, which is also found to be useful in other setups involving multiple robot parts, like bimanual manipulation [16].

We use RL to train our policy π by maximizing the discounted expected return $\mathbb{E}_\pi \left[\sum_{t=0}^{T-1} \gamma^t r_t\right]$, where r_t is the reward at time step t, γ is the discount factor, and T is the maximum episode length. The reward r is the sum of manipulation reward r^{manip} and locomotion reward r^{loco} as shown in Table 1. Notice that we use the second power of energy consumption at each leg joint to encourage both lower average and lower variance across all leg joints. We follow the simple reward design that encourages minimizing energy consumption from [17].

Command Vars	Training Ranges	Test Ranges
v_x^{cmd}	[0, 0.9]	[0.8, 1.0]
$\omega_{yaw}^{\text{cmd}}$	[-1,0, 1.0]	[-1, -.7] & [.7, 1]
l	[0.2, 0.7]	[0.6, 0.8]
p	$[-2\pi/5, 2\pi/5]$	$[-2\pi/5, 2\pi/5]$
y	$[-3\pi/5, 3\pi/5]$	$[-3\pi/5, 3\pi/5]$
T_{traj}	[1, 3]	[0.5, 1]

Table 2: Ranges for uniform sampling of command variables

We parameterize the end-effector position command p^{cmd} in spherical coordinate (l, p, y), where l is the radius of the sphere and p and y are the pitch and yaw angle. The origin of the spherical coordinate system is set at the base of the arm, but independent of torso's height, row and pitch (details in Supplementary). We set the end-effector pose command p^{cmd} by interpolating between the current end-effector position p and a randomly sampled end-effector position p^{end} every T_{traj} seconds:

Env Params	Training Ranges	Test Ranges
Base Extra Payload	[-0.5, 3.0]	[5.0, 6.0]
End-Effector Payload	[0, 0.1]	[0.2, 0.3]
Center of Base Mass	[-0.15, 0.15]	[0.20, 0.20]
Arm Motor Strength	[0.7, 1.3]	[0.6, 1.4]
Leg Motor Strength	[0.9, 1.1]	[0.7, 1.3]
Friction	[0.25, 1.75]	[0.05, 2.5]

Table 3: Ranges for uniform sampling of environment parameters

$$p_t^{\text{cmd}} = \frac{t}{T_{\text{traj}}} p + \left(1 - \frac{t}{T_{\text{traj}}}\right) p^{\text{end}}, \; t \in [0, T_{\text{traj}}].$$

p^{end} is resampled if any p_t^{cmd} leads to self-collision or collision with the ground. o^{cmd} is uniformly sampled from $\mathbb{SO}(3)$ space. Table 2 lists the ranges for sampling of all command variables.

2.1 Advantage Mixing for Policy Learning

Training a robust policy for a high-DoF robot is hard. In both manipulation and locomotion learning literature, researchers have used curriculum learning to ease the learning process by gradually increasing the difficulty of tasks so that the policy can learn to solve simple tasks first and then tackle difficult tasks [18, 19, 20]. However, most of these works require many manual tunings of a diverse set of the curriculum parameters and careful design of the mechanism for automatic curriculum.

Instead of introducing a large number of curricula on the learning and environment setups, we rely on only one curriculum with only one parameter to expedite the policy learning. Since we know that manipulation tasks are mostly related to the arm actions and locomotion tasks largely depends on leg actions, we can formulate this inductive bias in policy optimization by mixing advantage functions for manipulation and locomotion to speed up policy learning. Formally, for a policy with diagonal Gaussian noise and a sampled transition batch D, the training objective with respect to policy's parameters θ_π is

$$J(\theta_\pi) = \frac{1}{|\mathcal{D}|} \sum_{(s_t,a_t)\in\mathcal{D}} \log \pi(a_t^{\text{arm}} \mid s_t) \left(A^{\text{manip}} + \beta A^{\text{loco}}\right) + \log \pi(a_t^{\text{leg}} \mid s_t) \left(\beta A^{\text{manip}} + A^{\text{loco}}\right)$$

β is the curriculum parameter that linearly increases from 0 to 1 over timesteps T_{mix}: $\beta = \min(t/T_{\text{mix}}, 1)$. A^{manip} and A^{loco} are advantage functions based on r^{manip} and r^{loco} respectively. Intuitively, the Advantage Mixing reduces the credit assignment complexity by first attributing difference in manipulation returns to arm actions and difference in locomotion returns to leg actions, and then gradually anneal the weighted advantage sum to encourage learning arm and leg actions that help locomotion and manipulation respectively. We optimize this RL objective by PPO [21].

2.2 Regularized Online Adaptation for Sim-to-Real Transfer

Much prior work on Sim-to-Real transfer utilize the two-phase teacher-student scheme to first train a teacher network by RL using privileged information that is only available in simulation, and then the student network using onboard observation history imitates the teacher policy either in explicit action space or latent space [22, 23, 24, 25]. Due to the information gap between the full state available to the teacher network and partial observability of onboard sensories, the teacher network may provide supervision that is impossible for the student network to predict, resulting in a *realizability gap*. This problem is also noted in Embodied Agent community [26]. In addition, the second phase can only start after the convergence of the first phase, yielding extra burdens for both training and deployment.

To tackle the realizability gap and to remove the two-phase pipeline, we propose Regularized Online Adaptation (shown in Figure 2). Concretely, the encoder μ takes the privileged information e as input and predict an enviornment extrinsics latent z^μ for the unified policy to adapt its behavior in different environments. The adaptation module ϕ estimates the environment extrinsics latent z^ϕ by only condition on recent observation history from robot's onboard sensories. We jointly train μ with the unified policy π end-to-end by RL and regularize z^μ to avoid large deviation from z^ϕ estimated by the adaptation module. The adaption module ϕ is trained by imitating z^μ online. We formulate the loss function of the whole learning pipeline with respect to policy's parameters θ_π, privileged information encoder's parameters θ_μ, and adaptation module's parameters θ_ϕ as

$$L(\theta_\pi, \theta_\mu, \theta_\phi) = -J(\theta_\pi, \theta_\mu) + \lambda||z^\mu - \text{sg}[z^\phi]||_2 + ||\text{sg}[z^\mu] - z^\phi||_2 \ ,$$

where $J(\theta_\pi, \theta_\mu)$ is the RL objective discussed in Section 2.1, $\text{sg}[\cdot]$ is the stop gradient operator, and λ is the Laguagrian multiplier acting as regularization strength. The loss function can be minimized by using dual gradient descent: $\theta_\pi, \theta_\mu \leftarrow \arg\min_{\theta_\pi,\theta_\mu} \mathbb{E}_{(s,a)\sim\pi(\ldots,z^\mu)}[L]$, $\theta_\phi \leftarrow \arg\min_{\theta_\phi} \mathbb{E}_{(s,a)\sim\pi(\ldots,z^\phi)}[L]$, and $\lambda \leftarrow \lambda + \alpha \frac{\partial L}{\partial \lambda}$ with step size α. This optimization process is known to converge under mild conditions [27, 28]. In practice, we alternate the optimization process of the unified policy π and encoder μ and the one of adaptation module ϕ by a fixed number of gradient steps. λ increases from 0 to 1 by a fixed linear scheme. Notice that RMA [22] is a special case of Regularized Online Adaptation, in which the Laguagrian multiplier λ is set to be constant zero and the adaptation module ϕ starts training only after convergence of the policy π and the encoder μ.

	Survival ↑	Base Accel. ↓	Vel Error ↓	EE Error ↓	Tot. Energy ↓
Unified (Ours)	**97.1** $\pm$ 0.61	**1.00** $\pm$ 0.03	**0.31** $\pm$ 0.03	**0.63** $\pm$ 0.02	50 $\pm$ 0.90
Separate	92.0 $\pm$ 0.90	1.40 $\pm$ 0.04	0.43 $\pm$ 0.07	0.92 $\pm$ 0.10	51 $\pm$ 0.30
Uncoordinated	94.9 $\pm$ 0.61	1.03 $\pm$ 0.01	0.33 $\pm$ 0.01	0.73 $\pm$ 0.02	**50** $\pm$ 0.28

Table 4: Comparison of unified policy with separate policies for legs-arm, and one uncoordinated policy. The unified policy achieves the best performance given same energy consumption. The test ranges are in Table 2.

Deployment During deployment, the unified policy and adaptation module executes jointly onboard. To specify commands, we develop three interfaces: teleopertion by joysticks, closed-loop control by using RGB tracking, and open-loop reply of human demonstrations. Details are in Section 3.3.

3 Experimental Results

3.1 Robot System Setup

The robot platform is comprised of a Unitree Go1 quadraped [15] with 12 actuatable DoFs, and a robot arm which is the 6-DoF Interbotix WidowX 250s [29] with a parallel gripper. We mount the arm on top of the quadruped. The RealSense D435 provides RGB visual information and is mounted close to the gripper of WidowX. Both power of Go1 and WidowX are provided by Go1's onboard battery. Neural network inference is also done onboard of Go1. Our robot system uses only onboard computation and power so it is fully untethered.

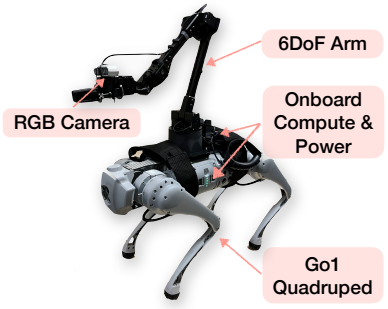

Figure 3: Robot system setup

3.2 Simulation Experiments

The purpose of our simulation experiments is to address the following questions:

- Does the unified policy improves over separate policies for the arm and legs? If so, how?
- How Advantage Mixing helps learning the unified policy?
- What's the performance of Regularized Online Adaptation compared with other Sim2Real methods?

Baselines and Metrics: We compare our method with the following baselines:

1. Separate policies for legs and the arm: one policy controls legs based on the quadraped observation, and another policy controls the arm based on arm observation.
2. One uncoordinated policy: Same as unified policy which observes aggregate state of base, legs and the arm, but only r^{manip} is used to train arm actions, and only r^{loco} for leg actions.
3. Rapid Motor Adaptation (RMA) [22]: Two-phase teacher-student baseline.
4. Expert policy: the unified policy using the privileged information encoder z^{μ}.
5. Domain Randomization: the unified policy trained without environment extrinsics z.

We report following metrics: (1) survival percentage, (2) Base Accel: angular acceleration of base, (3) Vel Error: L1 error between base velocity commands and actual base velocity, (4) EE Error: L1 error between end-effector (EE) command and actual EE pose, (5) Tot. Energy: total energy consumed by legs and the arm. All metrics are normalized by episode length. All experiments are tested over 3 randomly initialized networks and 1000 episodes each. Details of simulation and training are in Supplementary.

	Arm workspace (m^3) ↑	Survival under perturb ↑
Unified (Ours)	**0.82** $\pm$ 0.02	**0.87** $\pm$ 0.04
Separate	0.58 $\pm$ 0.10	0.64 $\pm$ 0.06
Uncoordinated	0.65 $\pm$ 0.02	0.77 $\pm$ 0.06

Table 5: In unified policy, legs help increase the arm workspace and the arm helps the quadruped to stabilize.

Improvements of the Unified Policy over Baselines: In Table 4, our unified policy outperforms separate and uncoordinated policies because both the arm and leg actions are trained with the sum of reward for manipulation and locomotion are given with observations for the arm, legs and the quadraped base, while baselines struggle to maintain a small base acceleration, which results in larger error in command velocity following and inaccurate EE pose following.

Unified Policy Increases Whole-body Coordination: Table 5 shows that our unified policy promotes whole-body coordination where (1) leg actions will help the arm to achieve a larger

	Realizability Gap $\|z^\mu - z^\phi\|_2$ ↓	Survival ↑	Base Accel. ↓	Vel Error ↓	EE Error ↓	Tot. Energy ↓
Domain Randomization	-	95.8 ± 0.2	**0.44** ± 0.00	0.46 ± 0.00	0.40 ± 0.00	**21.9** ± 0.53
RMA [22]	0.31 ± 0.01	95.2 ± 0.2	0.54 ± 0.02	0.44 ± 0.00	0.26 ± 0.04	27.3 ± 0.95
Regularized Online Adapt (Ours)	**2e-4** ± 0.00	**97.4** ± 0.1	0.51 ± 0.02	**0.39** ± 0.01	**0.21** ± 0.00	25.9 ± 0.56
Expert w/ Reg.	-	97.8 ± 0.2	0.52 ± 0.02	0.40 ± 0.01	0.21 ± 0.00	25.8 ± 0.49
Expert w/o Reg.	-	98.3 ± 0.2	0.51 ± 0.02	0.39 ± 0.00	0.21 ± 0.00	25.6 ± 0.30

Table 6: Regularized Online Adaptation outperforms other baselines with the smallest imitation error which helps it to have the same performance as the expert policy which uses privileged information to predict environment extrinsics. Expert policy trained with regularization term $\|z^\mu - \text{sg}[z^\phi]\|_2$ has negligible performance degradation compared with the expert trained without regularization. Test ranges in Table 3. Domain Randomization learns to just stand in most cases, hence, trivially collapsing to low Tot. Energy and Base Accel.

workspace via bending for lower EE commands and standing up high for higher EE commands, and (2) arm will help the robot balance under larger perturbation (1.0 m/s initial velocity of base) resulting in higher survival rate of the unified policy. We estimate the the arm workspace via calculating the volume of the convex hull of 1000 sampled EE poses, subtracted by the volume of a cube that encloses the quadruped.

Advantage Mixing Helps Learning the Unified Policy: Without Advantage Mixing, the unified policy has difficulty in credit assignment, resulting in the policy first learns EE command following but ignores the locomotion task. As shown in Figure 4, Advantage Mixing helps the policy to focus on each task first and then merge them together, which induces a curriculum-like mechanism to speed up training. Details in Supplementary.

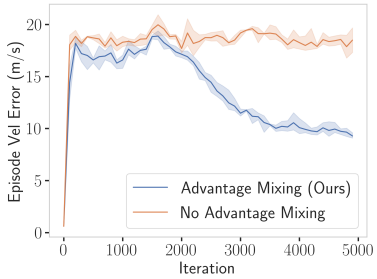

Figure 4: Advantage Mixing helps the unified policy to learn to follow the command velocity much faster (aggregated Vel Error over episodes decreases sharply) than without mixing.

Robust OOD Performance of Regularized Online Adaptation: We find that our Regularized Online Adaptation is more robust than RMA and Domain Randomization (DR), tested in environments with out-of-distribution (OOD) environment parameters in Table 3. In RMA, it is not guaranteed the estimated environment extrinsics by the adaptation module can imitates the one learned by the expert. With Regularized Online Adaptation, the expert learns to predict environment extrinsics with regularization from the adaptation module, thus tiny imitation error, **resulting in 20% reduction in EE Error**. Table 6 shows that adding regularization to expert has negligible negative impact on performance, while every metric gets improved compared to RMA due to smaller latent imitation error. Note that DR has better base acceleration and total energy as it just stands in place under difficult environments.

3.3 Real-World Experiments

We use the built-in Go1 MPC controller and the IK solver for operational space control of WidowX as the baseline in the real world, which we refer to as MPC+IK. More details are in the Supplementary.

Teleoperation: We specify EE position command p_t^{cmd} by parameterizing $p_{t+1}^{\text{cmd}} = p_t^{\text{cmd}} + \Delta p$, where $\Delta p = (\Delta l, \Delta p, \Delta y)$ is specified by two joysticks. With human in the loop, we can command the end-effector to reach points within or outside of training distribution. In Figure 5, we analyze the whole-body control in the real world, and show that the quadruped's base rotation $(r^{\text{quad}}, p^{\text{quad}}, y^{\text{quad}})$ strongly correlates with the EE position command p_t^{cmd}. This indicates that our unified policy enables whole-body coordination where the leg joints, as well as the arm joints, help reaching.

Vision-Guided Tracking: In addition to joystick control by humans, we also show successful picking tasks using visual feedback from an RGB camera. We mount a Realsense D435i camera near the gripper of the arm and use AprilTag [30] to get the relative position between the gripper and the object to be picked up. AprilTag is a visual fiducial system popular in robotics research using simple 2D black and white blocks to encode pose information. We first get the translation of the AprilTag in the camera frame $p^{\text{tag}} = [x^{\text{tag}}, y^{\text{tag}}, z^{\text{tag}}]^T$.

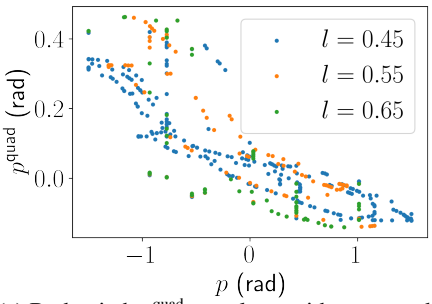

(a) Body pitch p^{quad} correlates with command EE pitch p with various lengths l.

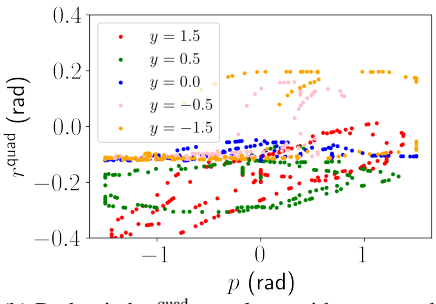

(b) Body pitch r^{quad} correlates with command EE pitch p with various yaws y.

Figure 5: Real-world whole-body control analysis. (a) We fix command EE yaw $y = 0$ and change command EE pitch p and length l. When p has a large magnitude, the quadruped will pitch upward or downward to help the arm reach for its goal. With larger l (goal far away), the quadruped will pitch more to help. (b) When the magnitude of command EE yaw y is closer to 1.578 (arm turns to a side of the torso), the quadruped will roll more to help the arm. When $y = 0$, the quadruped pitches downward instead of roll sideways to help the arm.

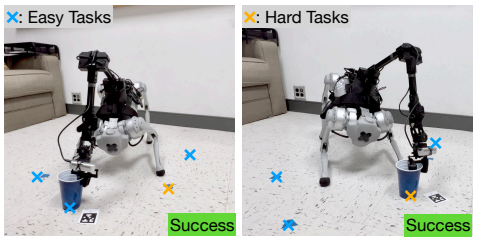

(a) Our method: success in both easy and hard tasks with coordinated behaviors.

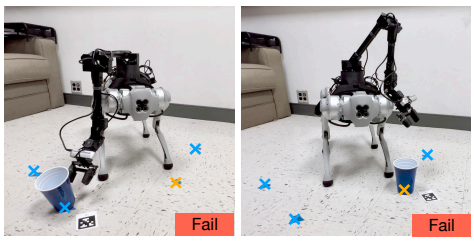

(b) MPC+IK: failure in both scenarios. Left: fail due to missed cup. Right: fail due to self-collision.

Figure 6: Comparison of our method and the baseline controller (MPC+IK) in vision-guided pick-up tasks. We sample different points around the robot as the target pick-up position. Easy tasks: 3 points are in normal distance from the robot. Hard tasks: when the point is very close to the front feet and are hard to reach without whole-body control. More hard tasks are in the Supplementary. Videos are at https://maniploco.github.io

Then we design and use a simple yet effective position feedback controller to set the current EE position command $p_t^{\text{cmd}} = K^T p^{\text{tag}}$, where $K = [-1.5, -1.5, 0.1]^T$ is a gain vector for position control. In Figure 6 and Table 7, we compare our method and the baseline (MPC+IK) in several pick-up tasks by measuring the success rate, average time to to completion (TTC), IK failure rate, and self-collision rate for every setting. We initialize the robot to the same default configuration and before execution.

	Success Rate ↑	TTC ↓	IK Failure Rate ↓	Self-Collision Rate ↓
Easy tasks (tested on 3 points)				
Ours	**0.8**	**5s**	-	**0**
MPC+IK	0.3	17s	0.4	0.3
Hard tasks (tested on 5 points)				
Ours	**0.8**	**5.6s**	-	**0**
MPC+IK	0.1	22.0s	0.2	0.5

Table 7: Comparison of our method v.s. MPC+IK on pick-up tasks. p^{end} is the goal position sampled from the points on the ground. TTC is the average time to completion. Each task performance is averaged on 10 real-world trials.

Analysis of Success and Failure Modes: Our method succeeds most of times on easy tasks without visible performance drop in hard task. The failed trials of our method are largely due to the mismatch between the actual cup position and the AprilTag position, which can be mitigated by using two AprilTags and averaging their poses (details in the Supplementary). Since the visual estimation is not the focus of this work, we infer that our method has higher precision and higher efficiency on pick-up tasks than MPC+IK. MPC+IK succeeds in some of the easy tasks and fails due to IK singularity or self-collision. In hard tasks, the major failure cause is self-collision given the cup is too close to the body. Notice that the TTC of MPC+IK is also longer than our method because solving online IK and operational space control more computationally demanding than joint position control (ours).

Open-loop Control from Demonstration: In this part, we analyze how agile walking is coupled with dynamic arm movement. The robot is given a pre-defined end-effector trajectory to follow in an open-loop manner while being commanded to walk at the same time. Results in Figure 7 show

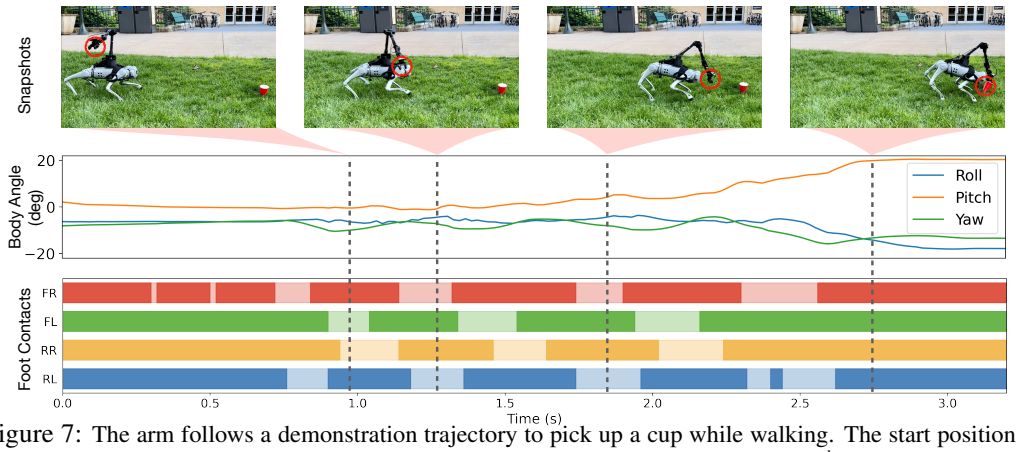

Figure 7: The arm follows a demonstration trajectory to pick up a cup while walking. The start position is $p = (0.5, -0.5, -1.2)$, at the right upper side of the robot and the end position is $p^{\text{end}} = (0.55, -0.9, 0.4)$, on the left lower front side close to the ground. $T_{\text{traj}} = 2.5s$. The robot initially stands on the ground and then is commanded by a constant forward velocity $v_x^{\text{cmd}} = 0.35$. Meanwhile the EE position command changes. When EE position command is high, the quadruped starts to walk without significant tilting behavior with a natural walking gait. As the EE position command moves below the torso, the quadruped starts to pitch downwards, roll to the left and yaw slightly to the right to help the arm reach the goal. Videos are at https://maniploco.github.io

agility and **dynamic coordination** of our legged manipulator on uneven grass terrain powered by our whole-body control method.

4 Related Work

Legged Locomotion Traditional model-based control methods for legged robots have shown success but often require controllers to be meticulously designed and many manual tunings [1, 2, 3, 4, 5, 31, 32, 33, 34, 35, 36, 6, 37]. The extra weight and movement of a robot arm on top of the legged robot will make such design process more challenging. Recent advances in reinforcement learning enable legged robots to traverse challenging terrains and adapt to changing dynamics [38, 24, 22, 39, 40, 41, 42, 43, 44, 45, 46, 47, 17, 48, 49, 50]. However these works only focus on the mobility part and few interactions with objects or the environment by manipulation are studied.

Mobile Manipulation Adding mobility to manipulation is studied in [51, 52, 53, 8, 54, 55, 10, 9, 56, 57, 58]. Advances have also been made in the field of biped humanoid [59, 60, 61, 62]. More recently, Ma et al. [8] proposed using an MPC controller to track the desired end-effector position of the arm mounted on a quadruped with a RL policy to maintain balance. However, the controllers for legs (RL) and arm (model-based) are separate modules and no dynamic movements are demonstrated. In [55], language models are used to guide a mobile robot to finish different tasks using the arm. However, the manipulation and mobility are utilized in a decoupled step-by-step manner.

5 Discussion and Limitations

We proposed a hardware setup as well as an algorithm to learn whole-body control of a legged robot with robotic arm. Our policy shows coordination between legs and arm while being able to control them in a dynamic manner. The method is trained fully in simulation and then transferred to the real-world using a learned adaptation strategy. We show the utility of our framework through teleoperation, visual tracking and open-loop control across several real-world tasks.

Limitations This work focuses on the whole-body control of a high-DoF mobile manipulator. Although we have shown preliminary results on object interaction (e.g. picking, pressing, erasing), incorporating general-purpose object interaction (e.g. grasping occluded scenes and soft object manipulation) into the our unified policy is a challenging open research direction. There are several ways in which the current methodology could be extended, such as, learning vision-based policies from the egocentric camera mounted on torso [63] and on the arm, climbing on the obstacle using front legs to pick something up on the table where the arm alone cannot reach, and etc. We believe this paper provides a first step towards several of such future directions.

Acknowledgments

We would like to thank Chris Atkeson for high-quality feedback, and Kenny Shaw, Russell Mendonca, Ellis Brown, Heng Yu, Unitree Robotics (Irving Chen, Yunguo Cui and Walter Wen) and staff at CMU Tech Spark for help in real-world experiments, hardware design and assembly. This work is supported in part by DARPA Machine Common Sense grant and ONR N00014-22-1-2096.

References

[1] H. Miura and I. Shimoyama. Dynamic walk of a biped. *IJRR*, 1984.

[2] M. H. Raibert. Hopping in legged systems—modeling and simulation for the two-dimensional one-legged case. *IEEE Transactions on Systems, Man, and Cybernetics*, 1984.

[3] H. Geyer, A. Seyfarth, and R. Blickhan. Positive force feedback in bouncing gaits? *Proceedings of the Royal Society of London. Series B: Biological Sciences*, 2003.

[4] K. Yin, K. Loken, and M. Van de Panne. Simbicon: Simple biped locomotion control. *ACM Transactions on Graphics*, 2007.

[5] K. Sreenath, H.-W. Park, I. Poulakakis, and J. W. Grizzle. A compliant hybrid zero dynamics controller for stable, efficient and fast bipedal walking on mabel. *IJRR*, 2011.

[6] M. Hutter, C. Gehring, D. Jud, A. Lauber, C. D. Bellicoso, V. Tsounis, J. Hwangbo, K. Bodie, P. Fankhauser, M. Bloesch, et al. Anymal-a highly mobile and dynamic quadrupedal robot. In *IROS*, 2016.

[7] L. Sentis and O. Khatib. A whole-body control framework for humanoids operating in human environments. In *ICRA*, 2006.

[8] Y. Ma, F. Farshidian, T. Miki, J. Lee, and M. Hutter. Combining learning-based locomotion policy with model-based manipulation for legged mobile manipulators. *RA-L*, 2022.

[9] C. D. Bellicoso, K. Krämer, M. Stäuble, D. Sako, F. Jenelten, M. Bjelonic, and M. Hutter. Alma-articulated locomotion and manipulation for a torque-controllable robot. In *ICRA*, 2019.

[10] S. Zimmermann, R. Poranne, and S. Coros. Go fetch!-dynamic grasps using boston dynamics spot with external robotic arm. In *ICRA*, 2021.

[11] N. Bernstein. The co-ordination and regulation of movements. *The co-ordination and regulation of movements*, 1966.

[12] M. L. Latash. The bliss (not the problem) of motor abundance (not redundancy). *Experimental brain research*, 217(1):1–5, 2012.

[13] M. Bruton and N. O'Dwyer. Synergies in coordination: a comprehensive overview of neural, computational, and behavioral approaches. *Journal of Neurophysiology*, 120(6):2761–2774, 2018.

[14] B. Dynamics. Spot Arm. https://www.bostondynamics.com/.

[15] X. Wang. Unitree go1. https://www.unitree.com/products/go1/.

[16] S. Kataoka, S. K. S. Ghasemipour, D. Freeman, and I. Mordatch. Bi-manual manipulation and attachment via sim-to-real reinforcement learning. *arXiv preprint arXiv:2203.08277*, 2022.

[17] Z. Fu, A. Kumar, J. Malik, and D. Pathak. Minimizing energy consumption leads to the emergence of gaits in legged robots. In *CoRL*, 2021.

[18] G. B. Margolis, G. Yang, K. Paigwar, T. Chen, and P. Agrawal. Rapid locomotion via reinforcement learning. *RSS*, 2022.

[19] N. Rudin, D. Hoeller, P. Reist, and M. Hutter. Learning to walk in minutes using massively parallel deep reinforcement learning. In *CoRL*, 2022.

[20] I. Akkaya, M. Andrychowicz, M. Chociej, M. Litwin, B. McGrew, A. Petron, A. Paino, M. Plappert, G. Powell, R. Ribas, et al. Solving rubik's cube with a robot hand. *arXiv preprint arXiv:1910.07113*, 2019.

[21] J. Schulman, F. Wolski, P. Dhariwal, A. Radford, and O. Klimov. Proximal policy optimization algorithms. *arXiv:1707.06347*, 2017.

[22] A. Kumar, Z. Fu, D. Pathak, and J. Malik. RMA: Rapid Motor Adaptation for Legged Robots. In *RSS*, 2021.

[23] G. B. Margolis, T. Chen, K. Paigwar, X. Fu, D. Kim, S. bae Kim, and P. Agrawal. Learning to jump from pixels. In *CoRL*, 2021.

[24] J. Lee, J. Hwangbo, L. Wellhausen, V. Koltun, and M. Hutter. Learning quadrupedal locomotion over challenging terrain. *Science Robotics*, 2020.

[25] T. Miki, J. Lee, J. Hwangbo, L. Wellhausen, V. Koltun, and M. Hutter. Learning robust perceptive locomotion for quadrupedal robots in the wild. *Science Robotics*, Jan. 2022.

[26] L. Weihs, U. Jain, I.-J. Liu, J. Salvador, S. Lazebnik, A. Kembhavi, and A. Schwing. Bridging the imitation gap by adaptive insubordination. *NeurIPS*, 2021.

[27] S. Levine, C. Finn, T. Darrell, and P. Abbeel. End-to-end training of deep visuomotor policies. *JMLR*, 2016.

[28] H. Wang and A. Banerjee. Bregman alternating direction method of multipliers. *NeurIPS*, 2014.

[29] WidowX 250 robot arm 6DOF - X-Series robotic arm. https://www.trossenrobotics.com/widowx-250-robot-arm-6dof.aspx.

[30] E. Olson. AprilTag: A robust and flexible visual fiducial system. In *Proceedings of the IEEE International Conference on Robotics and Automation (ICRA)*, pages 3400–3407. IEEE, May 2011.

[31] A. M. Johnson, T. Libby, E. Chang-Siu, M. Tomizuka, R. J. Full, and D. E. Koditschek. Tail assisted dynamic self righting. In *Adaptive Mobile Robotics*. World Scientific, 2012.

[32] M. Khoramshahi, H. J. Bidgoly, S. Shafiee, A. Asaei, A. J. Ijspeert, and M. N. Ahmadabadi. Piecewise linear spine for speed–energy efficiency trade-off in quadruped robots. *Robotics and Autonomous Systems*, 2013.

[33] A. D. Ames, K. Galloway, K. Sreenath, and J. W. Grizzle. Rapidly exponentially stabilizing control lyapunov functions and hybrid zero dynamics. *IEEE Transactions on Automatic Control*, 2014.

[34] D. J. Hyun, J. Lee, S. Park, and S. Kim. Implementation of trot-to-gallop transition and subsequent gallop on the mit cheetah i. *IJRR*, 2016.

[35] M. Barragan, N. Flowers, and A. M. Johnson. MiniRHex: A small, open-source, fully programmable walking hexapod. In *RSS Workshop*, 2018.

[36] G. Bledt, M. J. Powell, B. Katz, J. Di Carlo, P. M. Wensing, and S. Kim. Mit cheetah 3: Design and control of a robust, dynamic quadruped robot. In *IROS*, 2018.

[37] C. S. Imai, M. Zhang, Y. Zhang, M. Kierebinski, R. Yang, Y. Qin, and X. Wang. Vision-guided quadrupedal locomotion in the wild with multi-modal delay randomization. *arXiv:2109.14549*, 2021.

[38] J. Hwangbo, J. Lee, A. Dosovitskiy, D. Bellicoso, V. Tsounis, V. Koltun, and M. Hutter. Learning agile and dynamic motor skills for legged robots. *Science Robotics*, 2019.

[39] Z. Li, X. Cheng, X. B. Peng, P. Abbeel, S. Levine, G. Berseth, and K. Sreenath. Reinforcement learning for robust parameterized locomotion control of bipedal robots. In *ICRA*, 2021.

[40] X. B. Peng, E. Coumans, T. Zhang, T.-W. E. Lee, J. Tan, and S. Levine. Learning agile robotic locomotion skills by imitating animals. In *RSS*, 2020.

[41] W. Yu, J. Tan, C. K. Liu, and G. Turk. Preparing for the unknown: Learning a universal policy with online system identification. In *RSS*, 2017.

[42] W. Yu, C. K. Liu, and G. Turk. Policy transfer with strategy optimization. In *ICLR*, 2018.

[43] W. Zhou, L. Pinto, and A. Gupta. Environment probing interaction policies. In *ICLR*, 2019.

[44] W. Yu, V. C. V. Kumar, G. Turk, and C. K. Liu. Sim-to-real transfer for biped locomotion. In *IROS*, 2019.

[45] W. Yu, J. Tan, Y. Bai, E. Coumans, and S. Ha. Learning fast adaptation with meta strategy optimization. *RA-L*, 2020.

[46] X. Song, Y. Yang, K. Choromanski, K. Caluwaerts, W. Gao, C. Finn, and J. Tan. Rapidly adaptable legged robots via evolutionary meta-learning. In *IROS*, 2020.

[47] I. Clavera, A. Nagabandi, S. Liu, R. S. Fearing, P. Abbeel, S. Levine, and C. Finn. Learning to adapt in dynamic, real-world environments through meta-reinforcement learning. In *ICLR*, 2019.

[48] L. Smith, J. C. Kew, X. B. Peng, S. Ha, J. Tan, and S. Levine. Legged robots that keep on learning: Fine-tuning locomotion policies in the real world. In *ICRA*, 2022.

[49] R. Yang, M. Zhang, N. Hansen, H. Xu, and X. Wang. Learning vision-guided quadrupedal locomotion end-to-end with cross-modal transformers. In *ICLR*, 2022.

[50] Z. Fu, A. Kumar, A. Agarwal, H. Qi, J. Malik, and D. Pathak. Coupling vision and proprioception for navigation of legged robots. In *CVPR*, 2022.

[51] C. Sun, J. Orbik, C. M. Devin, B. H. Yang, A. Gupta, G. Berseth, and S. Levine. Fully autonomous real-world reinforcement learning with applications to mobile manipulation. In *CoRL*, 2022.

[52] J. Wong, A. Tung, A. Kurenkov, A. Mandlekar, L. Fei-Fei, S. Savarese, and R. Martín-Martín. Error-aware imitation learning from teleoperation data for mobile manipulation. In *CoRL*, 2022.

[53] D. Honerkamp, T. Welschehold, and A. Valada. Learning kinematic feasibility for mobile manipulation through deep reinforcement learning. *RA-L*, 2021.

[54] X. Ding and F. Yang. Study on hexapod robot manipulation using legs. *Robotica*, 34(2): 468–481, Feb. 2016.

[55] M. Ahn, A. Brohan, N. Brown, Y. Chebotar, O. Cortes, B. David, C. Finn, K. Gopalakrishnan, K. Hausman, A. Herzog, D. Ho, J. Hsu, J. Ibarz, B. Ichter, A. Irpan, E. Jang, R. J. Ruano, K. Jeffrey, S. Jesmonth, N. J. Joshi, R. Julian, D. Kalashnikov, Y. Kuang, K.-H. Lee, S. Levine, Y. Lu, L. Luu, C. Parada, P. Pastor, J. Quiambao, K. Rao, J. Rettinghouse, D. Reyes, P. Sermanet, N. Sievers, C. Tan, A. Toshev, V. Vanhoucke, F. Xia, T. Xiao, P. Xu, S. Xu, and M. Yan. Do as I can, not as I say: Grounding language in robotic affordances. 2022.

[56] F. Xia, C. Li, R. Martín-Martín, O. Litany, A. Toshev, and S. Savarese. Relmogen: Leveraging motion generation in reinforcement learning for mobile manipulation. *arXiv preprint arXiv:2008.07792*, 2020.

[57] K. Dong, K. Pereida, F. Shkurti, and A. P. Schoellig. Catch the ball: Accurate high-speed motions for mobile manipulators via inverse dynamics learning. In *IROS*, 2020.

[58] K. Blomqvist, M. Breyer, A. Cramariuc, J. Förster, M. Grinvald, F. Tschopp, J. J. Chung, L. Ott, J. Nieto, and R. Siegwart. Go fetch: Mobile manipulation in unstructured environments. *ICRA Workshop*, 2020.

[59] S. Kuindersma, R. Deits, M. Fallon, A. Valenzuela, H. Dai, F. Permenter, T. Koolen, P. Marion, and R. Tedrake. Optimization-based locomotion planning, estimation, and control design for the atlas humanoid robot. *Autonomous robots*, 2016.

[60] S. Feng, E. Whitman, X. Xinjilefu, and C. G. Atkeson. Optimization based full body control for the atlas robot. In *International Conference on Humanoid Robots*, 2014.

[61] J. Chestnutt, M. Lau, G. Cheung, J. Kuffner, J. Hodgins, and T. Kanade. Footstep planning for the honda asimo humanoid. In *ICRA*, 2005.

[62] N. A. Radford, P. Strawser, K. Hambuchen, J. S. Mehling, W. K. Verdeyen, A. S. Donnan, J. Holley, J. Sanchez, V. Nguyen, L. Bridgwater, et al. Valkyrie: Nasa's first bipedal humanoid robot. *Journal of Field Robotics*, 2015.

[63] A. Agarwal, A. Kumar, J. Malik, and D. Pathak. Legged locomotion in challenging terrains using egocentric vision. In *Conference on Robot Learning (CoRL)*, 2022.

[64] V. Makoviychuk, L. Wawrzyniak, Y. Guo, M. Lu, K. Storey, M. Macklin, D. Hoeller, N. Rudin, A. Allshire, A. Handa, and Gavriel State. Isaac gym: High performance GPU-Based physics simulation for robot learning. Aug. 2021.

A Experiment Videos

We perform thorough real-world analysis of our framework and our custom-built legged manipulator. We urge the reader to look at the compiled result videos at https://maniploco.github.io . As we can see in the video, legs and arm function in coordination with each other where legs bend and stretch to increase the reach of the arm as well as to attain stability.

B Regularized Online Adaptation Details

Algorithm 1 Regularized Online Adaptation

Randomly initialize privileged information encoder μ, adaptation module ϕ, unified policy π
Initialize with empty replay buffer D
for $itr = 1, 2, \ldots$ **do**
  for $i = 1, 2, \ldots, N_{env}$ **do**
    $s_0, e_0 \leftarrow$ envs[i].reset()
    for $t = 0, 1, \ldots, T$ **do**
      if itr mod $H == 0$ **then**
        $z_t^{\phi} \leftarrow \phi(s_{t-10:t-1}, a_{t-11:t-2})$
        $a_t \leftarrow \pi((s_t, a_{t-1}, z_t^{\phi}))$
      else
        $z_t^{\mu} \leftarrow \mu(e_t)$
        $a_t \leftarrow \pi((s_t, a_{t-1}, z_t^{\mu}))$
      end if
      $s_{t+1}, r_t \leftarrow$ envs[i].step(a_t)
      Store $((s_t, e_t), a_t, r_t, (s_{t+1}, e_{t+1}), z_t^{\phi}, z_t^{\mu})$ in D
    end for
  end for
  if itr mod $H == 0$ **then**
    Update θ_{ϕ} by optimizing $||\text{sg}[z_t^{\mu}] - z_t^{\phi}||_2$
  else
    Update $\theta_{\pi}, \theta_{\mu}$ by optimizing $-J(\theta_{\pi}, \theta_{\mu}) + \lambda||z_t^{\mu} - \text{sg}[z_t^{\phi}]||_2$, where $J(\theta_{\pi}, \theta_{\mu})$ is the advantage mixing RL objective in Section 2.1 of the main paper
  end if
  Empty D
  $\lambda \leftarrow$ Linear_Curriculum(itr)
end for

We presented the details of Regularized Online Adaptation (Section 2.2 of the main paper) in Algorithm 1. We set H to be 20. The regularization coefficient λ follows a linear curriculum which starts at 0 and stops at 1: $\lambda = \min(\max(\frac{itr-5000}{5000}, 0), 1)$.

C Simulation Details

We obtained URDF files for the quadraped and the robot arm from Unitree and Interbotix separately. We customized the URDF files to connect the two parts rigidly. Shown in Figure 8, we use Nvidia's IsaacGym [64] for parallel simulation. We use fractal noise to generate the terrain. The parameters for the fractual noise are number of octaves = 2, fractal lacunarity = 2.0, fractal gain = 0.25, frequency = 10Hz, amplitude = 0.15m. We found that the generated rough terrain will enforce foot clearance and replace the complex rewards that are needed if flat terrain is used for simulation [38].

We sample an EE position command by first sampling a spherical coordinate (l, p, y) from Table 2 of the main paper. Then world coordinate of p^{end} is obtained as $T(\text{S2C}[(l, p, y)]) + (p_x^{\text{base}}, p_y^{\text{base}}, p_z^{\text{base}})$, where T is the linear transformation according to the base orientation, S2C[] is the operator to transform spherical coordinates to Cartesian coordinates, and p^{base} is the base position. To encourage

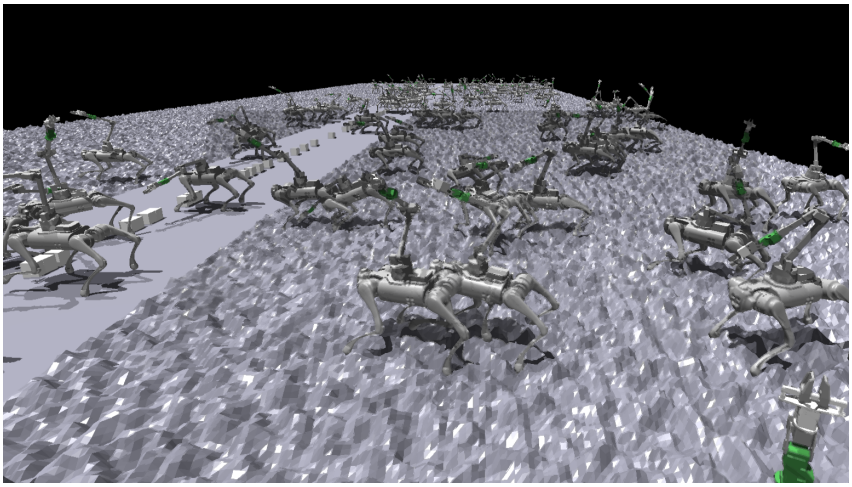

Figure 8: Customized simulation environment based on IsaacGym

smooth arm motion and whole-body coordination, we set p_z^{base} to be a constant (0.53) and row and pitch in T to be 0, so EE position commands are z, row, pitch-independent of the base.

We simulate each episode for a maximum of 1000 steps and terminate the episode earlier if the height of the robot drops below 0.28m, body roll angle exceeds 0.2 radians if EE position command if on the left of the body base ($p_{\text{y}}^{\text{cmd}} > 0$) , or is less than -0.2 radians if EE position command is on the right of the body base ($p_{\text{y}}^{\text{cmd}} < 0$), or the body pitch exceeds 0.2 radians if EE position command is above body base ($p_{\text{p}}^{\text{cmd}} > 0$), or is less than -0.2 radians if EE position command is below body base ($p_{\text{p}}^{\text{cmd}} < 0$). We do not early terminate if the arm self-collide and any body parts with the terrain, but the EE command positions are sampled in a way that

The control frequency of the policy is 50Hz, and the simulation frequency is 200Hz. We set the stiffness (K_p) for leg joints and arm joints to be 50 and 5 respectively and the damping (K_d) to be 1 and 0.5 respectively. The default target joint positions for leg joints are $[-0.1, 0.8, -1.5, 0.1, 0.8, -1.5, -0.1, 0.8, -1.5, 0.1, 0.8, -1.5]$ and for arm joints are zeros. The delta range of target joint positions for leg joints is 0.45 and for arm joints are $[2.1, 1.0, 1.0, 2.1, 1.7, 2.1]$.

D Training Details

The policy is a multi-layer perceptron which takes in the current state $s_t \in \mathbb{R}^{75}$, which is concatenated with the environment extrinsics $z_t \in \mathbb{R}^{20}$. The first hidden layer has 128 dimensions and after that the network splits into 2 heads, where each has 2 hidden layers of 128 dimensions. The outputs of two heads are concatenated, where the leg actions $a_t^{\text{leg}} \in \mathbb{R}^{12}$ and arm actions $a_t^{\text{arm}} \in \mathbb{R}^6$. We train

Table 8: Training Hyper-parameters

PPO clip range	0.2
Learning rate	2e-4
Reward discount factor	0.99
GAE λ	0.95
Number of environments	5000
Number of environment steps per training batch	40
Learning epochs per training batch	5
Number of mini-batches per training batch	4
Minimum policy std	0.2

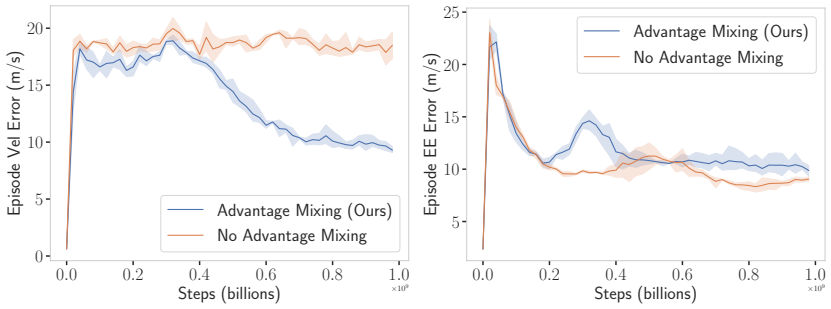

Figure 9: Advantage mixing helps the unified policy to learn to walk and grasp at the same time. Without Advantage Mixing, the unified policy fails to learn to walk where the Episode Vel Error (episodic sum of L1 error between velocity commands and current velocities) is constantly high. In this case, the unified policy stays at local minima of only following EE commands.

for 10000 iterations / training batches, which are 2 billions of samples and 200k gradient updates. We list the hyperparameters of PPO [21] in Table 8 of the Supplementary.

E Advantage Mixing Details

For a policy with diagonal Gaussian noise and a sampled transition batch D, the training objective with respect to policy's parameters θ_π is

$$
\begin{aligned}
J(\theta_\pi) &= \frac{1}{|\mathcal{D}|} \sum_{(s_t,a_t)\in\mathcal{D}} \log \pi\left(a_t \mid s_t\right) A(s_t, a_t) \\
&= \frac{1}{|\mathcal{D}|} \sum_{(s_t,a_t)\in\mathcal{D}} \log \left(\pi(a_t^{\text{arm}} \mid s_t)\pi(a_t^{\text{leg}} \mid s_t)\right) \left(A^{\text{manip}}(s_t, a_t) + A^{\text{loco}}(s_t, a_t)\right) \\
&\rightarrow \frac{1}{|\mathcal{D}|} \sum_{(s_t,a_t)\in\mathcal{D}} \log \pi(a_t^{\text{arm}} \mid s_t) \left(A^{\text{manip}} + \beta A^{\text{loco}}\right) + \log \pi(a_t^{\text{leg}} \mid s_t) \left(\beta A^{\text{manip}} + A^{\text{loco}}\right)
\end{aligned}
$$

In Figure 9 of the Supplementary, we plot the episodic velocity command following error (Episode Vel Error) and EE comand following error (Episode EE Error) against number of steps during training. Advantage mixing helps the unified policy to learn to walk and grasp at the same time. Without Advantage Mixing, the unified policy fails to learn to walk where the Episode Vel Error (episodic sum of L1 error between velocity commands and current velocities) is constantly high. In this case, the unified policy stays at local minima of only following EE commands by not exploring in leg action space, since the initial exploration phase in leg action space will destabilize the base which harms manipulation tasks.

F Real-World Setup and Experiment Details

Table 9: Camera Parameters for Vision Tracking

Resolution	640 × 400
Frequency	10 Hz
Tag/Cam offset	(-0.02, -0.03, 0.12)

The robot platform is comprised of a Unitree Go1 quadraped [15] with 12 actuatable DoFs, and a robot arm which is the 6-DoF Interbotix WidowX 250s [29] with a parallel gripper. We mount the arm on top of the quadruped. The RealSense D435 provides RGB visual information and is mounted close to the gripper of WidowX. Both power of Go1 and WidowX (60 Watts) are provided by Go1's battery.

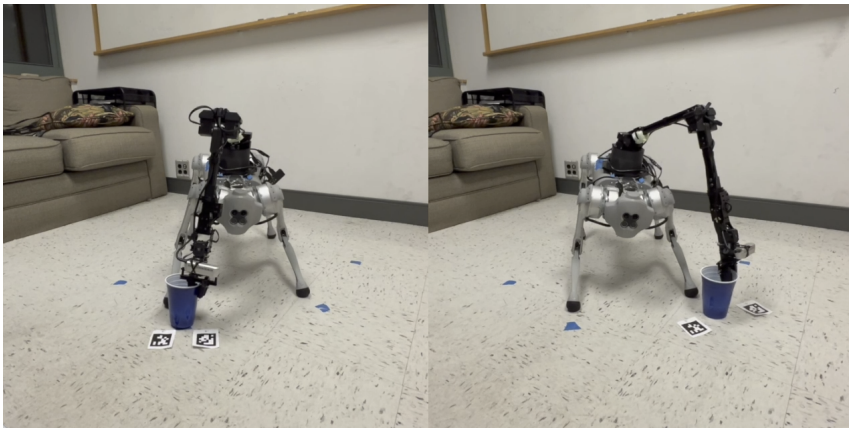

Figure 10: Vision-guided tracking by using the average pose of the two AprilTags as the target pose.

	Ground Points (p^{end})	Success Rate ↑	TTC ↓	IK Failure Rate ↓	Self-Collision Rate ↓
Easy tasks (tested on 3 points)					
Ours	$\begin{bmatrix}(0.62,-1.27,-1.11)\\(0.57,-1.16,0.55)\\(0.58,-1.14,1.78)\end{bmatrix}$	**0.8**	**5s**	-	**0**
MPC+IK		0.3	17s	0.4	0.3
Hard tasks (tested on 5 point)					
Ours	$\begin{bmatrix}(0.72,-0.51,0.34)\\(0.55,-0.75,-0.43)\\(0.56,-0.73,0.5)\\(0.45,-0.74,1.80)\\(0.45,-0.76,-1.8)\end{bmatrix}$	**0.8**	**5.6s**	-	**0**
MPC+IK		0.1	$22.0s$	0.2	0.5

Table 10: Comparison of our method v.s. MPC+IK on pick-up tasks. p^{end} is the goal position sampled from the points on the ground. TTC is the average time to tompletion. All data are averaged on 10 real-world trials.

In real-world experiments, we directly deploy the unified policy with the adaptation module with weights fixed onto the onboard computation of Go1, both modules operate at 50Hz. The inference of policy and adaption module are done on Raspberry Pi 4. The software stack of the WidowX 250s arm is setup on Nvidia TX2 by using the official codebase at https://github.com/Interbotix/interbotix_ros_manipulators. UDP is used as the communication protocal between Pi and TX2. EE gripper closing and opening are not a part of the policy.

In teleoperation experiments, the gripper action is directly controlled by a joystick controller. In vision-guided tracking experiments, we use a scripted policy to control the gripper: when the gripper position is close to the desired position specified by the AprilTag [30] for 1 second, the gripper closes; otherwise, it keeps open.

We listed the camera parameters used in vision-guided tracking in Table 9 of the Supplementary. The "Tag/Cam offset" describes what the desired translation of the tag should be viewed in the camera frame when using the position controller to specify desired end-effector position in spherical coordinate. Shown in Figure 10 of the Supplementary, we also performed additional experiments on vision-guided tracking suggested by Reviewer bkQw by using two AprilTags and averaging their pose to get the target pose. Video results are at here. We listed the positions of ground points for visual-guided tracking tasks in Table 10. More results on hard tasks are at here.